Original Article

Exposure to zinc oxide nanoparticles affects testicular structure, reproductive development and spermatogenesis in parental and offspring male rats

Xinyu Hong[1#^], Naimin Shao[2#], Lei Yin[3], Chen Li[2], Gonghua Tao[2], Yuli Sun[2], Kelei Qian[2], Jun Yang[2], Ping Xiao[2], Xiaozhong Yu[4], Zhijun Zhou[1]

[1]School of Public Health, Fudan University, Shanghai, China; [2]Shanghai Municipal Center for Disease Control and Prevention/State Environmental Protection Key Laboratory of Environmental Health Impact Assessment of Emerging Contaminants, Shanghai, China; [3]Reprotox Biotech LLC, Albuquerque, New Mexico, USA; [4]College of Nursing, University of New Mexico, Albuquerque, New Mexico, USA

Contributions: (I) Conception and design: X Hong, P Xiao, X Yu, Z Zhou; (II) Administrative support: None; (III) Provision of study materials or patients: None; (IV) Collection and assembly of data: None; (V) Data analysis and interpretation: N Shao, L Yin, C Li, G Tao, K Qian, J Yang; (VI) Manuscript writing: All authors; (VII) Final approval of manuscript: All authors.

[#]These authors contributed equally to this work.

Correspondence to: Ping Xiao. Shanghai Municipal Center for Disease Control and Prevention/State Environmental Protection Key Laboratory of Environmental Health Impact Assessment of Emerging Contaminants, 1380 Zhongshan West Road, Shanghai 200336, China.
Email: xiaoping@scdc.sh.cn; Xiaozhong Yu. College of Nursing, University of New Mexico, 2502 Marble Avenue, Albuquerque 87131, New Mexico, USA. Email: xiyu@salud.unm.edu; Zhijun Zhou. School of Public Health, Fudan University, 130 Dong'an Road, Shanghai 200032, China.
Email: zjzhou@shmu.edu.cn.

Background: This study aimed to comprehensively evaluate the toxicity exerted by zinc oxide nanoparticles (ZnO NPs) on rat testis and its effects on fertility and progeny development.

Methods: Different concentrations of ZnO NPs were administered by gavage to Sprague Dawley (SD) rats to examine the adverse effects resulting from pre- and post-natal exposure. Systemic distribution of ZnO NPs, developmental performance, sperm parameters, reproductive performance, histopathological examination, and sex hormone levels were determined scheduled in the experimental rats and their male offspring. The comparative *in vitro* cytotoxicity of the ZnO NPs was determined among C18-4, TM3, and TM4 cells. The toxicity exerted by ZnO NPs on germ cells *in vitro* and the effects on the expression of cytoskeleton and blood-testis barrier (BTB)-related proteins were also determined.

Results: After oral gavage, ZnO NPs mainly accumulated in the liver and testes of rats; 350 mg/kg ZnO NPs adversely affected the epididymal weight, sperm motility, and hormone levels but did not affect the fertility of rats. In addition, 350 mg/kg ZnO NPs significantly reduced the reproductive and developmental performance of offspring male rats. Testicular histopathological and electron microscopic ultrastructure examinations showed more significant abnormal structural changes than those observed in parental rats. The results of *in vitro* cell experiments further showed that ZnO NPs exerted cytotoxic effects on germ cells, and led to DNA damage, nucleoskeleton and cytoskeleton alterations, and could regulate actin changes through changes in LC3B.

Conclusions: It is possible that ZnO NPs act directly on TM4 cells by penetrating the BTB, causing damage to the cytoskeleton and disrupting the dynamic balance of the BTB, thereby destroying the microenvironment necessary for spermatogenesis, which may lead to poor reproduction in rats.

Keywords: ZnO nanoparticles; testis toxicity; blood-testis barrier (BTB); TM4 cells; fertility

^ ORCID: 0000-0002-1298-1585.

Submitted May 20, 2022. Accepted for publication Jul 07, 2022.
doi: 10.21037/atm-22-3047
View this article at: https://dx.doi.org/10.21037/atm-22-3047

Introduction

In recent years, nanotechnology has developed rapidly in various fields of human life such as biomedicine, industry, agriculture, food, cosmetics, and so on (1-3). Nanoparticles (NPs) are compounds or particles between 1 and 100 nanometres in size. The properties of NPs are mainly related to their nanoscale structure, size and structure-related electronic configurations and their extremely large surface to volume ratio relative to bulk materials (4). NPs enter the body mainly through the respiratory system and, because of their extremely small size, can penetrate cell membranes to enter cells or pass through cells and transfer to other parts of the body. It has been shown that NPs are deposited in the respiratory tract and alveoli of animals, which leads to alveolar macrophage damage (5). Zinc oxide nanoparticles (ZnO NPs) are among the most commonly used nanomaterials. They have unique physical and chemical attributes such as antibacterial and UV absorption properties, and are widely used in food additives, medicines, cosmetics, and other fields (6,7). Due to their wide applications, human are exposed to ZnO NPs in daily life, and they enter the body by the oral route, inhalation, and injection administration. Accumulation in organs may be potentially toxic to human health (8,9). Therefore, it is necessary to evaluate the potential effects of ZnO NPs in organisms.

As we all know, zinc is one of the necessary trace elements for humans; it is widely present in all tissues of the human body, and participates in the regulation of macromolecular biosynthesis and cellular processes (10,11). Furthermore, zinc is necessary for sperm formation and maturation and is the main component of semen (12). However, recent studies have shown that ZnO NPs damages the cytoskeleton and changes the nuclear envelope (NE), leading to reactive oxygen species (ROS) accumulation, culminating in apoptotic cell death (13,14). Han *et al.* showed that ZnO NPs have the potential to induce apoptosis in testicular cells likely through DNA damage caused by reactive oxygen species, with possible adverse consequences for spermatogenesis and therefore, male fertility (15). The ZnO NPs were shown to cause DNA damage in a mouse Sertoli cell line (TM4) model *in vitro*, and down-regulated the expression of blood-testis barrier (BTB) protein (16). Rafiee *et al.* (17) detected degenerative changes in testicular tissues in mice after oral administration of ZnO NPs, but there was no apparent damage in Leydig cells and Sertoli cells. However, it was found that ZnO NPs were cytotoxic in mouse testicular Leydig TM3 cells, causing increased steroid production and inducing cell apoptosis (18). These *in vivo* and *in vitro* studies have demonstrated that the special properties of nanomaterials may have potential testicular harmful effects, but there is not enough epidemiological or animal experimental evidence. Therefore, it is necessary to evaluate the possible reproductive health risks caused by exposure to ZnO NPs.

We conducted an extended one-generation reproductive toxicity study comprising investigation of the distribution of nano-zinc oxide in the testis of F_0 male rats. The pathological changes of testicular tissue, measurement of testosterone, luteinizing hormone (LH), and follicle-stimulating hormone (FSH) levels, and sperm count and motility were included. Furthermore, changes in mating and pregnancy outcomes in paired maternal rats and effects on the male reproductive system of F_1 offspring rats were also included in detail. Moreover, *in vitro* comparison of cytotoxicity among testicular cells including C18 spermatogonia cell, TM3 Leydig cell and TM4 Sertoli cells as well as high content image-based examination of cytoskeletal alteration and BTB-related proteins in TM4 cell were conducted to explore the underlining mechanism of the effect of nano-zinc oxide on testicular spermatogenesis. We present the following article in accordance with the ARRIVE reporting checklist (available at https://atm.amegroups.com/article/view/10.21037/atm-22-3047/rc).

Methods

Chemicals

We obtained ZnO NPs (20 nm) from Nanostructured & Amorphous Materials, Inc. (Houston, TX, USA); ZnO NPs (50 nm), micro ZnO (<5 μm), Dulbecco's modified Eagle's medium (DMEM), penicillin-streptomycin solution, phosphate-buffered saline (PBS), bovine serum albumin (BSA), neutral red (NR), and 3-(4,5-dimethylthiazol-2-

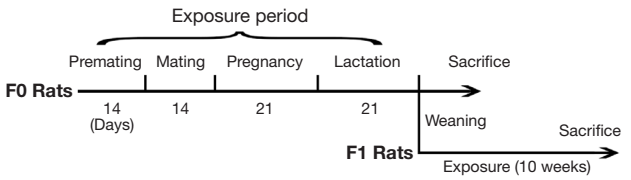

Figure 1 Schematic study design—extended one-generation reproductive toxicity study. Before mating, parental F_0 generation rats were administered ZnO NPs (1 mL/100 g bw) by intragastric gavage continuously for 2 weeks. Then, males and females were bred 1:2 for 2 weeks until positive evidence of mating was found (the vaginal smear had vaginal plug or sperm). Subsequently, the males and females were separated and kept in a single cage. F_1 males and females assigned to Cohort 1A were bred in a similar manner as the F_0 generation, and females were allowed to rear their litters normally until weaning on PND21, when 1 pup/sex/litter was assigned to constitute the F_2 generation. Since this experiment only studied the toxicity related to the male reproductive system, the offspring rats only retain the Cohort 1A. ZnO NPs, zinc oxide nanoparticles; PND, postnatal day.

yl)-2,5-diphenyl tetrazolium bromide (MTT) were all purchased from Sigma-Aldrich (St. Louis, MO, USA). Horse serum and DMEM/F12 were purchased from Hyclone (Logan, UT, USA). Nu-Serum was purchased from BD Bio Sciences (Becton, Dickinson, and Co., Franklin Lakes, NJ, USA). Fetal bovine serum (FBS) was purchased from Gibco (Grand Island, NY, USA). Hematoxylin and eosin (HE) were obtained from Shanghai Hongzi Industrial Co., Ltd. (Shanghai, China). Glucose, sodium chloride, absolute ethanol, 75% ethanol, xylene, hydrochloric acid, lithium nitrate, glutaraldehyde, and osmium tetroxide were all analytically pure and purchased from Shanghai Lingfeng Chemical Reagent Co., Ltd. (Shanghai, China). We purchased 96% ethanol and glacial acetic acid from Merck & Co Inc. (Kenilworth, NJ, USA).

Characterization of ZnO NPs

ZnO NPs particle size analysis

The ZnO NPs were dissolved in ethanol and then dropped on carbon-coated copper grid and dried overnight at room temperature. Finally, a transmission electron microscope (TEM; JEM-2100, JEOL, Tokyo, Japan) and Image J software (National Institutes of Health, Bethesda, MD, USA) were used to characterize the shape and size of ZnO NPs.

ZnO NPs hydrated particle size and stability analysis

The ZnO NPs particles were dissolved in 0.5% glucose solution and FBS to make a suspension (35 mg/mL). Subsequently, dynamic light scattering (DLS) was used to analyze the hydrated particle size and Zeta potential of the ZnO NPs on the first and seventh days after preparation. The mixture was subjected to ultrasonication at 25 ℃ for 30 seconds. The DLS characterization of ZnO NPs in cell test solution (20 μg/mL) was same as methods described above.

Animals

A total of 60 male and 120 female Sprague Dawley (SD) rats (13-week-old) were purchased from Beijing Victory Laboratory Animal Technology Co., Ltd (SCXK; Beijing, China, 2016-0011). Female rats were nulliparous and non-pregnant. All animals were housed in the animal room of the Shanghai Municipal Center for Disease Control and Prevention (SYXK; Shanghai, China, 2013-0008). The room temperature was maintained at 20–26 ℃ with an artificially illuminated 12-hour dark/light cycle and relative humidity of 40–70%. The rats were fed with a commercial diet (Beijing Keao Xieli Feed Co., Ltd., Beijing, China) and water ad libitum.

Extended one-generation reproductive toxicity study

An extended one-generation reproductive toxicity experiment was conducted following the Organization for Economic Co-operation and Development (OECD) 2018 test guideline 443 (19) as illustrated in *Figure 1*. Briefly, the rats were randomly divided into 4 groups (15 males or 30 females per group) after 5 days of acclimatization. These groups were exposed to the following dosages of ZnO NPs: 0 (control group), 7 mg/kg bw, 50 mg/kg bw, and 350 mg/kg bw groups for 2 weeks before mating and continuously through mating, gestation, and pup weaning (F_1 generation) (20). This study focused on the evaluation of male reproductive and developmental effects that may occur as a result of pre- and postnatal exposure on the offspring males (1A cohort offspring rats) as well as an assessment of testicular toxicity on the F_0 males. At weaning, 20 male and female pups are selected and assigned to cohorts of animals for reproductive/developmental toxicity testing. The F_1 offspring received further treatment with the ZnO NPs from weaning to full maturity (age of 13 weeks).

Clinical observations and pathology examinations were performed on all animals for signs of toxicity, with special emphasis on the integrity and performance of the male and female reproductive systems (F_0) and the health, growth, development, and function of the offspring. At the time of termination as indicated in *Figure 1*, 6 rats in each group were weighed and anesthetized with sodium pentobarbital (60 mg/kg bw), and blood was taken immediately from the abdominal aorta for serum biochemical analysis. Following necropsy, tissues and organs were collected for assessment of organ weight, zinc concentration, and histopathological analysis. Sperm count and motility, as well as morphology, were evaluated for all males (F_0 parent males and F_1 male offspring). Animal experiments were performed in accordance with the Guide for the Care and Use of Laboratory Animals (21). The animal experiment protocol was reviewed and approved by the Animal Ethics Review Committee of the Shanghai Municipal Center for Disease Control and Prevention. A protocol was prepared before the study without registration.

Zinc content in liver and testis

The determination of zinc levels in the liver and left testis were quantified by using inductively coupled plasma-mass spectrometry (ICP-MS) (7700x; Agilent Technologies, Santa Clara, CA, USA). Briefly, the free-dried samples were placed in concentrated nitric acid overnight for pre-digestion. Subsequently, they were digested with a microwave digestion apparatus (Mars6; CEM Corporation, Matthews, NC, USA). Then, they were placed on an electric heating plate at 100 ℃ for 30–60 minutes, and the final volume was brought to 10 mL. Finally, ICP-MS was performed to analyze the zinc concentration.

Serum sample collection and serum biochemical analysis

The blood was centrifuged for 15 minutes at 2,000 rpm to collect serum which was used for the detection of Testosterone (T), follicle-stimulating hormone (FSH), and luteinizing hormone (LH) levels according to the enzyme-linked immunosorbent assay (ELISA) manufacturer's instructions (Shanghai Enzyme link Biotechnology Co., Ltd., Shanghai, China). The absorbance was recorded at 505 nm with a microplate reader (Thermo Fisher Scientific, Waltham, MA, USA) and using the established standard curve from the ELISA kit to obtain the hormone levels.

Organ weights, histopathology, and electron microscopic ultrastructure

The liver and testis were removed, subjected to necroscopic analysis, and weighted to determine the wet weight of each organ. The relative organ weight was then calculated for each organ (organ weight/body weight).

Next, the left testis of 9 rats in each group were randomly selected to fix in 10% neutral formalin, and then the organs were embedded in paraffin and sliced into 4 μm thick sections. Finally, these sections were stained with HE and examined under the light microscope.

In addition, part of the right testes of the rats was taken and fixed in Bouin's solution (Phygene, China) for 18 hours. Then, the Bouins solution was replaced with 10% neutral formalin and the tissues were fixed twice for 24 hours each time. Finally, the organs were stained with Schiff and hematoxylin, the cross-section of the seminiferous tubules was observed and photographed under an oil microscope.

The other part of right testes was fixed in 10% glutaric acid (pH=7.2–7.4), and post-fixed in osmium tetroxide. Then, ethanol and acetone were used for gradient dehydration. The samples were embedded in epoxy resin and hardened at room temperature for 16 hours. Subsequently, sections were stained with uranyl acetate and lead nitrate. Finally, testis's ultrastructure was observed and pictures were taken with a TEM.

Quantification of the cellular composition of spermatogenic cells in the seminiferous tubules

The stages of the rats' cycle were classified according to the stipulations of Ichihara *et al.* (22). We randomly selected 12 VII seminiferous tubules from the testis tissue of each rat under an optical microscope. Spermatogonia, pre-thin-line spermatocytes, thick-line stage spermatocytes, round spermatids, and the nuclei of Sertoli cells were counted in each seminiferous tubule. The mean values of 12 seminiferous tubules were treated as the representative value of each animal.

Analysis of the chemical composition of nanoparticles in the testis

Energy dispersion analysis of X-ray (EDX) spectroscopy with Helios G4 plasma focused ion beam (FIB) system was performed on the prepared testicular electron microscope observation samples to further confirm whether the particles

photographed in the TEM of the testis were ZnO NPs.

Analysis of sperm count, motility, and morphology in male rats

To assess the number, vitality, and morphology of the sperm, the left epididymis was quickly separated to prepare a sperm suspension. Then, 4 drops of the sperm suspensions were pipetted onto the glass slide and the proportion of motile sperm was observed under a microscope (Nikon eclipse 80; Tokyo, Japan). We observed 10 visual fields for each animal and the average number of dead sperm (500 sperm per field) and the number of dead sperm were also calculated.

The number of sperm was counted under a microscope. A 0.5 mL sperm suspension was taken and diluted with 9.5 mL of saline, and then a 10 μL sperm suspension was transferred into a hemocytometer and stood for 5 minutes.

A drop of the sperm suspension was taken and fixed with methanol for 5 minutes and stained with 1% eosin for 1 hour. Then, the sperm morphology was observed under the microscope after washing and the types of shape of sperm were counted. A total of 1,000 sperm per animal were counted and the deformity rate (%) was calculated. All studies were performed in triplicate.

Evaluation of reproductive performance in F_0 rats

Males and females were bred 1:2 in the cage and allowed to mate for 2 weeks as described by Turnbull *et al.* (23). The females were checked every day through vaginal smear to determine whether they had completed mating. If sperm were found in the smear, it indicated that the mating was successful, and this day was identified as GD 0. The parturition day of females was confirmed as postnatal day (PND) 0, and then the live and stillborn pups were scored. The non-pregnant female rats were immediately sacrificed, and the uterus was stained with 10% ammonium sulfide to confirm whether there were implantation sites. Reproductive performance was summarized in terms of pregnant animal rats, conception rate, and pregnancy rate.

F_1 offspring males

The F_1 animals were assigned to Cohort 1A. Their survival and sex were determined on PND1; body weights were recorded on PND1, 4, 7, 14, and 21. The anogenital distance (AGD) of each male pup was measured on PND4, and normalized with the weight of the pup that day. After PND21, 1 female pup and 1 male pup from each offspring were selected to be treated with ZnO NPs and to observe their mating, conception, and pregnancy. The method of obtaining the body weights, organ weights, histopathological examination of testis, sperm parameters, and serum sex hormones of offspring males was the same as that of the parental rats.

Cell culture and cell treatment

The mouse C18-4 spermatogonia cell line was obtained from Professor Marie-Claude Hofmann (The University of Texas MD Anderson Cancer Center, Houston, TX, USA). The C18-4 cell line was cultured in DMEM medium supplemented with 5% FBS and 100 U/mL penicillin-streptomycin at 33 ℃ in a humidified incubator with 5% CO_2. The C18-4 cells were passaged every 3–4 days, and cells used in all experiments were below 7 passages. The mouse Leydig cells (TM3) and Sertoli cells (TM4) were purchased from American Type Culture Collection (ATCC; Manassas, VA, USA). Then, cells were cultured in DMEM/F12 medium supplemented with 5% horse serum, 2.5.% FBS, and 100 U/mL penicillin-streptomycin at 37 ℃ in a humidified incubator with 5% CO_2. The TM3 and TM4 cells were passaged every 2 days and cells used in all experiments were below 8 passages. The cultured cells were treated with different concentrations and periods of ZnO NPs.

Cell viability assay

To compare cytotoxicities of ZnO NPs, the cell viabilities of C18-4, TM3, and TM4 cells were measured by neutral red assay (NR), and the half half-maximal inhibitory concentration (IC_{50}) was calculated after treatment with ZnO NPs (24). Briefly, C18-4, TM3, and TM4 cells were seeded in 96-well plates (1.5×10^4 cells/well) and cultured overnight at 70–80% confluence. After washing with PBS, the cells were incubated with ZnO NPs for 24 or 48 hours. Then, the culture medium was removed and the fresh medium containing NR (50 μg/mL) was added. After 3 hours of incubation, cells were washed twice with PBS and 200 μL of eluent was added to each well. Then, the absorbance at 540 nm was determined by a microplate reader (Bng Labtech, Cary, NC, USA). Each assay was repeated 6 times. The IC_{50} was calculated by JMP 13.0 statistical analysis package (SAS Institute, Cary, NC, USA)

In the present study, we chose TM4 cells for further experiments as ZnO NPs were more toxic to them according to the results of NR. The MTT assay was performed to evaluate the effects of ZnO NPs and micro ZnO on the viability of TM4 cells. The TM4 cells were treated with different concentrations of ZnO NPs (1, 2, 5, and 10 μg/mL) or micro ZnO (1, 10, and 100 μg/mL) for 24 and 48 hours. A total of 20 μL MTT (5 mg/mL) was added to each well. Then, the culture solutions were aspirated carefully and added 150 μL dimethyl sulfoxide (DMSO). The absorbance at 490 nm was measured by a microplate reader.

Immunofluorescence staining

The TM4 cells were incubated with different concentrations of ZnO NPs (0, 0.2, 0.5, 0.75, 1.0, and 1.25 μg/mL) for 24 and 48 hours. Then, cells were fixed with 4% paraformaldehyde for 20 minutes at room temperature. Fixed cells were blocked with 0.1% Triton X-100 (Merck, USA) and 3% BSA in PBS for 30 minutes after permeabilizing by 0.1% Triton X-100 in Triton/PBS solution for 15 minutes. Subsequently, cells were incubated with rabbit anti-LC3B (1:100) (Thermo Fisher Scientific, USA), mouse anti-Arp3 (1:50) (Sigma-Aldrich, USA), mouse anti-α-tubulin (1:300) (Abcam, USA), and rabbit γ-H2AX (1:200) (Millipore-Sigma, Burlington, MA, USA) in 0.1% TX-100/PBS overnight at 4 ℃. After washing twice with 0.05% Tween-20/PBS, cells were incubated with goat anti-mouse Dylight 650 (1:1,000) (Thermo Fisher Scientific, USA), goat anti-rabbit Dylight 550 (1:1,000) (Thermo Fisher Scientific, USA) and the DNA staining dye Hoechst 33342 (Molecular Probes, Eugene, OR, USA) in PBS/BSA for 90 minutes at room temperature in the dark, followed by incubation with 50 μL Alexa Fluor 488 Phalloidin (Cell Signaling Technology, Danvers, MA, USA) per well at room temperature for 30 minutes for F-actin staining.

High-content imaging analysis

The changes in nuclear morphology were determined by high-content imaging analysis (HCA) according to the previous study (24). Briefly, the HCS Studio TM 2.0 Target Activation BioApplication (Thermo Fisher, USA) was used to analyze multi-channel images. A total of 49 fields per well were acquired at 40× magnification using Hamamatsu ROCA-ER digital camera (Hamamatsu, Japan) combined with 0.63× coupler and Carl Zeiss microscope (ZEISS, Oberkochen, Germany) optics in auto-focus mode.

Single-cell based HCA provided multi-parameters to characterize various parameters from each cell quantitatively. Nuclear shape measurement included P2A and LWR parameters. Total intensity was defined as total pixel intensities within a cell in the respective channel. With 49 fields of each well, at least 4,000 cells were analyzed per well, and single-cell-based data for each channel were exported for further statistical analysis. The experiments were performed with at least 4 biological replicates and repeated twice.

Association analysis of BTB-related proteins

In order to further analyze the structure distribution and correlation of BTB-related microglobulin, tubulin, and ankyrin, we obtained the high-resolution photos of each channel from an ArrayScan VTI HCS reader (Thermo Fisher, USA), and imported into an open-source software CellProfiler and CellProfiler Analyst (Broad Institute, Cambridge, MA, USA). We classified and measured multi-parameters, including the size, shape, intensity, texture of F-actin and LC3B, Arp3, and α-tubulin.

Statistical analysis

All data obtained from HCS Studio 2.0 BioApplication and Cellprofiler were exported to JMP 13.0 statistical analysis package (SAS Institute, Cary, NC, USA) for further analysis. Objects with a nuclear area less than 50 μM^2 or larger than 800 μM^2 were excluded to remove cell debris and clumps. The γ-H2AX positive cells were set by the total intensity of γ-H2AX in control over 120, 000 pixels. The parameters based on single-cell imaging were quantified and used to determine the geometric mean of each well. Data were presented as geometric mean ± SD. One-way analysis of variance (ANOVA) was used to determine statistical significance ($P<0.05$) followed by Tukey-Kramer all pairs comparison.

The IC_{50} value was calculated using the logic 4P model in the Sigmoid curve conforming to JMP.

To check the relationship between BTB-related proteins, Spearman correlation analysis was performed after the logarithmic transformation of the obtained data.

Results

Characterization of ZnO NPs

In this study, TEM and DLS were used to characterize ZnO

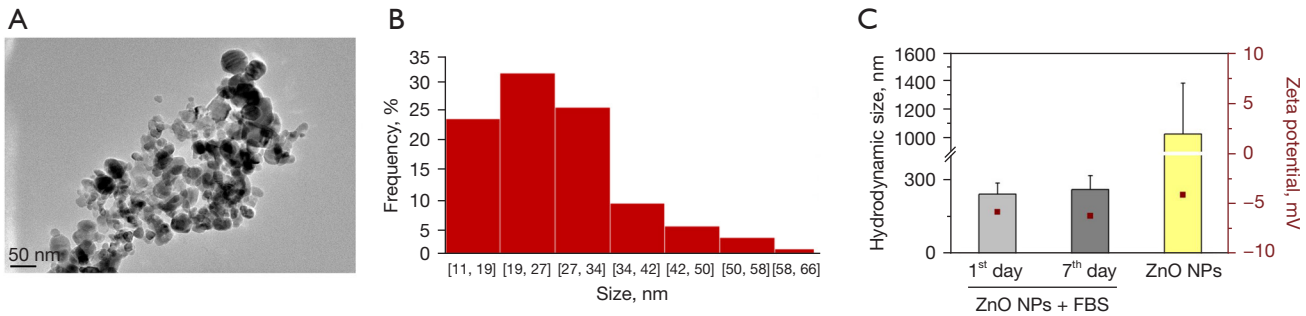

Figure 2 The characterization of ZnO NPs. (A) The TEM image of ZnO NPs. (B) The size distribution of ZnO NPs. (C) The zeta potential and particle size of ZnO NPs. ZnO NPs, zinc oxide nanoparticles; TEM, transmission electron microscope.

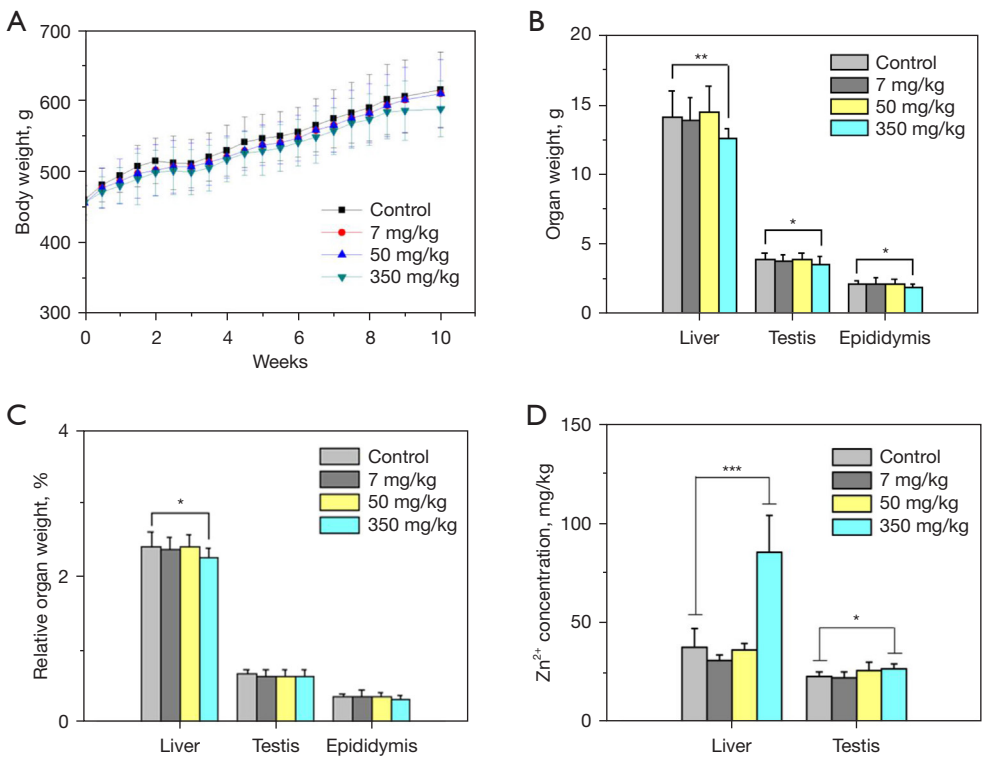

Figure 3 Body and tissues weights and Zinc element concentration. (A) Body weight of male SD rats after 70 days oral administration of ZnO NPs. (B) Organ weights of male SD rats. (C) Organ coefficient of male SD rats. Organ coefficient = organ weight/weight at the end of the experiment × 100%. (D) The concentration of Zinc in liver and testis of male SD rats. Statistical significance is represented as *P<0.05, **P<0.01 and ***P<0.001 as compared with control group. ZnO NPs, zinc oxide nanoparticles; SD, Sprague-Dawley.

NPs (*Figure 2*). The TEM image results showed that the shape of ZnO NPs was granular, with an average particle size of around 26.60 nm (*Figure 2A*). The average hydrodynamic diameter of ZnO NPs was about 11–34 nm (*Figure 2B*). Subsequently, the particle size distribution of 35 mg/mL ZnO NPs with DLS determination demonstrated that ZnO NPs have a certain degree of agglomeration. However, they could still be maintained in a smaller particle size range, and the stability was good within 7 days (*Figure 2C*).

Body and tissues weights and Zinc element concentration

There were no apparent symptoms of toxicity, but the body weight of experimental group rats increased during

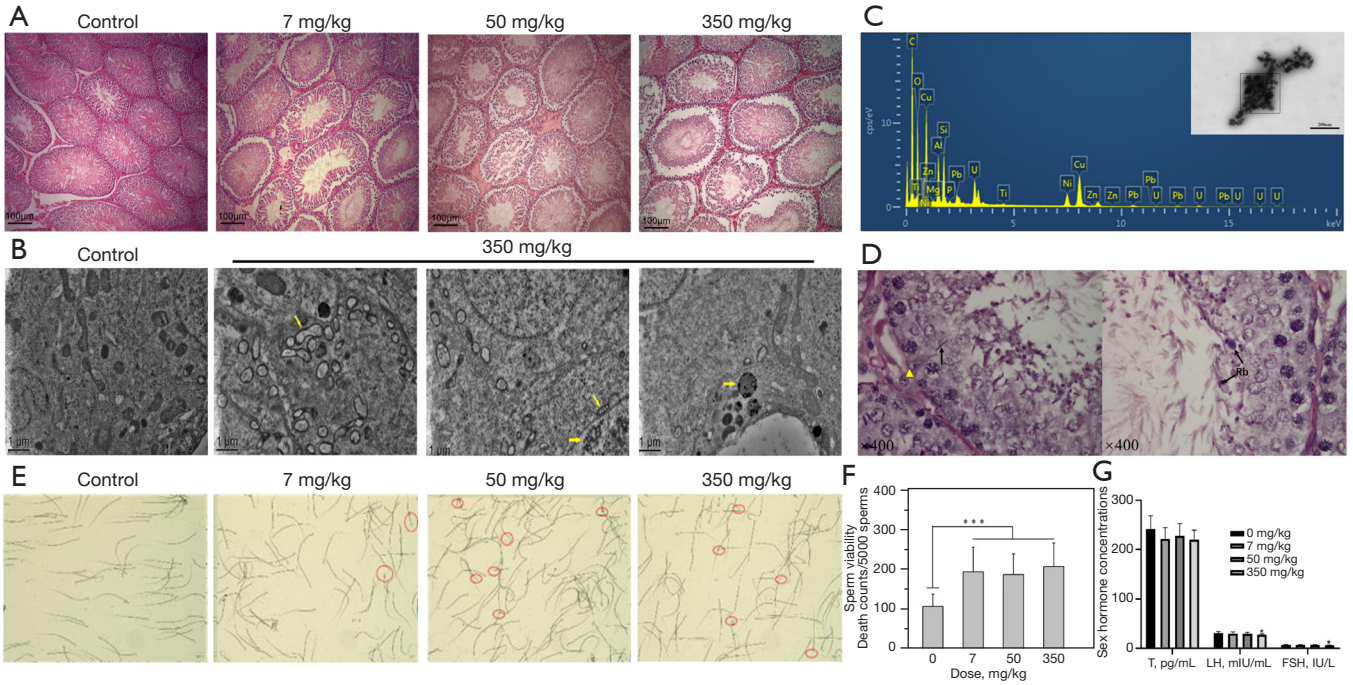

Figure 4 The sperm parameters, sex hormone levels, and testicular histopathological evaluation of F_0 generation. (A) Light microscopy of cross-sections of HE-stained testes from male SD rats (×200). (B) TEM images of ZnO NPs internalization by testes (×400). The yellow arrows in the 350 mg/kg group indicate swelling and vacuolation of mitochondria, destruction of mitochondrial ridges and nuclear lysis, and a large number of late lysosomes in the cytoplasm. (C) EDX spectroscopy detected whether the particles in the TEM image were ZnO NPs. (D) Light microscopy of cross-sections of PAS-stained testes from male SD rats (×400). The arrow on the left is the elongated spermatozoa retained in the seminiferous layer; ▲, The cytoplasm of the supporting cell is vacuolated; Rb: the sperm cell remnant near the lumen surface. (E) Light microscopy of morphology of dead sperms from male SD rats. The red circle shows abnormal sperm morphology, which mainly includes headless, hookless and ring-shaped tail. (F) Number of dead sperms in the left epididymis. (G) Hormone levels (T, LH and FSH) in serum of male rats detected by ELISA. Statistical significance is represented as *P<0.05 and ***P<0.001 as compared with control group. ZnO NPs, zinc oxide nanoparticles; SD, Sprague-Dawley; HE, hematoxylin and eosin; EDX, energy dispersion analysis of X-ray; TEM, transmission electron microscope; PAS, periodic acid-Schiff; ELISA, enzyme-linked immunosorbent assay. T, testosterone; LH, luteinizing hormone; FSH, follicle-stimulating hormone.

treatments (*Figure 3A*). Moreover, with the prolongation of the treatment, the weight gain of rats in the 350 mg/kg group began to slow down, but there was no statistical difference compared with the control group (P>0.05). Compared with the control group, the organ weights of testis, liver, and epididymis in the 350 mg/kg group were significantly reduced (P<0.05) (*Figure 3B*). *Figure 3C* suggests that the organ coefficients of each dose group also showed a downward trend, and the organ coefficients of the liver were significantly decreased in the 350 mg/kg group. Interestingly, the Zinc element concentration in the liver and testis in the 350 mg/kg group was significantly increased (P<0.05) (*Figure 3D*).

Histopathological evaluation

We used HE staining, TEM, and periodic acid-Schiff (PAS) staining to conduct the histopathological examination of male rat testis. The results of HE showed that testis sections of the control group showed normal histological architecture, while the ZnO NPs treatment groups had different degrees of interstitial swelling, shedding of seminiferous layer, atrophy, and necrosis of seminiferous tubules, and necrosis of sperm cells (*Figure 4A*).

Subsequently, we further observed the testicular tissue by TEM (*Figure 4B*). The results revealed that mitochondrial swelling and vacuolization, and loose and disordered internal

Table 1 F_1 generation (Cohort 1A)—sperm parameters and reproductive performance

Test Items	ZnO NPs (mg/kg bw/d)			
	0	7	50	350
Sperm parameters (mean ± SD)				
Sperm survival (%)	96.3±1.1	95.2±0.8*	93.3±0.7**	91.8±0.7**
Dead sperm (pcs/5,000)	183.6±53.3	233.5±39.5**	335.9±36.5**	410.5±34.1**
Spermatid count (10^7/g)	1.93±0.42	1.86±0.93	1.69±0.83*	1.64±0.92*
Reproductive performance				
Mating male rat count	8	8	8	8
Mating female rat count	16	16	16	16
Pregnant female mouse count	10	10	14	9
Delivery rat	9	10	14	7
Have implantation sites before childbirth	1	0	0	2
Dystocia	0	0	0	0
Conception rate (%)	62.5	62.5	87.5	56.2*
Pregnancy rate (%)	90	100	100	77.78*

Statistical significance is represented as *P<0.05 and **P<0.01 as compared with control group. ZnO NPs, zinc oxide nanoparticles.

ridges had occurred in the testicular cells in the 350 mg/kg ZnO NPs group. Lysosomes and heterochromatin in the nucleus increased, and sperm cell mitochondrial sheath degraded (Figure S2). In addition, we also found granular agglomerates of suspected ZnO NPs of testicular tissue in the 350 mg/kg ZnO NPs group. Therefore, to further confirm that the particles photographed in TEM were ZnO NPs, EDX spectroscopy was performed on the prepared testicular samples (*Figure 4C*). The results showed that the testicular tissue contained Zn, O, C, and Cu elements. Since the peak spectra of Cu and Zn were very close, it was not possible to distinguish them from the ion concentration values shown in Table S1. The results of EDX could still show that the particles found in the testis were ZnO NPs, which indicates that the ZnO NPs can penetrate the BTB to enter the testicular cells.

Furthermore, we performed PAS staining on the testis to determine the seminiferous epithelial cycle. *Figure 4D* shows that in the seminiferous tubules without necrosis, the arrangement of spermatogenic cells was disordered and the Sertoli cells were vacuolated. Elongated sperm cells were retained in the seminiferous epithelium during the VII-VIII developmental stages. Each selected rat exhibited VII 12 stage seminiferous epithelium without apparent necrosis under the light microscope. There was no significant effect detected on the spermatogenesis (P>0.05) (Table S2).

Sperm parameters and reproductive performance in F_0 generation

The changes of sperm parameters after ZnO NPs exposure in the control group and each dose group of male rats are shown in *Table 2* and *Figure 4E,4F*. The results showed that the sperm survival rate decreased with the increase of ZnO NPs dose (P<0.01). The number of dead sperms increased significantly in a dose-dependent manner (P<0.01). In addition, there was no effect of ZnO NPs exposure on F_0 reproductive performance (P>0.05) (*Table 2*). The levels of T, LH, and FSH in F_0 male rats decreased with the increase of ZnO NPs dose, and the levels of LH and FSH in the 350 mg/kg ZnO NPs group were significantly different from those in the control group (P<0.05) (*Figure 4G*).

Developmental and reproductive toxicity assessments in F_1 generation

The F_1 animals designed for developmental and reproductive toxicity assessments were assigned to Cohort 1A. *Figure 5A* demonstrates that average male pup body weight was lowest in the 350 mg/kg ZnO NPs group during PND 14–21

Table 2 F_0 generation—male sperm parameters and reproductive performance

Test Items	ZnO NPs (mg/kg bw/d)			
	0	7	50	350
Sperm parameters (mean ± SD)				
Sperm motility (%)	97.8±1.1	96.1±2.4*	96.2±1.8*	95.8±1.9**
Dead sperm count (pcs/5,000)	107.8±31.1	195.2±62.1**	188.3±52.5**	208.8±59.6**
Sperm count (10^7/g epididymis)	1.77±0.62	1.67±0.45	2.00±0.89	2.35±0.54
Sperm deformities count (pcs/1,000)	88	115	150	110
Type of deformity				
Head deformity	22	14	27	26
Headless	59	90	88	69
Tail deformity	7	11	35	15
Reproductive performance				
Mating male rat count	15	15	15	15
Mating female rat count	30	30	30	30
Pregnant female mouse count	16	19	19	15
Delivery rat	12	16	19	15
Have implantation sites before childbirth	4	3	2	3
Dystocia	0	0	1	0
Conception rate (%)	53.33	66	73.33	60
Pregnancy rate (%)	75	84.21	86.36	83.33

Statistical significance is represented as *P<0.05 and **P<0.01 as compared with control group. ZnO NPs, zinc oxide nanoparticles.

(P<0.05), and the weight-standardized AGD value in male pups decreased significantly in a dose-dependent manner (P<0.05) (*Figure 5B*).

Subsequently, the offspring were weighed twice a week after weaning. The results showed that the offspring body weight in 350 mg/kg ZnO NPs group was significantly lower than the control group in the third week and from halfway through the 6th week to the 13th week (P<0.05) (*Figure 5C*). As shown in *Table 3*, organ weights showed that except for the lungs, other organ weights were significantly lower than those of the control group (P<0.05). However, there was no significant difference in the organ coefficients of each dose group compared with the control group (P>0.05), which indicates that the reduction of organ weight was related to the bodyweight loss.

The analysis results of sperm parameters showed that compared with the control group, the sperm survival decreased significantly in a dose-dependent manner (P<0.05) (*Table 1*). Similarly, the dead sperm increased significantly in a dose-dependent manner (P<0.01). In addition, the sperm counts of rats in the 50 and 350 mg/kg ZnO NPs groups were significantly lower than that of the control group (P<0.05). Through histopathological examination, it was found that the testicular interstitium of the offspring rats had obvious edema and inflammatory infiltration (*Figure 5D*). Compared with the parental rats, the seminiferous epithelium was further shedding. Even in the 50 and 350 mg/kg ZnO NPs groups, the seminiferous epithelium completely shed into the lumen, and the sperm cells in each stage were extensively decreased, accompanied by a decrease in lumen diameter. However, ZnO NPs exposure had no significant effect on the LH and FSH levels of offspring male rats, but the T levels in the 50 and 350 mg/kg ZnO NPs groups were significantly lower than that in the control group (P<0.05) (*Figure 5E*). In addition, the conception and pregnancy rates in the 350 mg/kg ZnO NPs group were

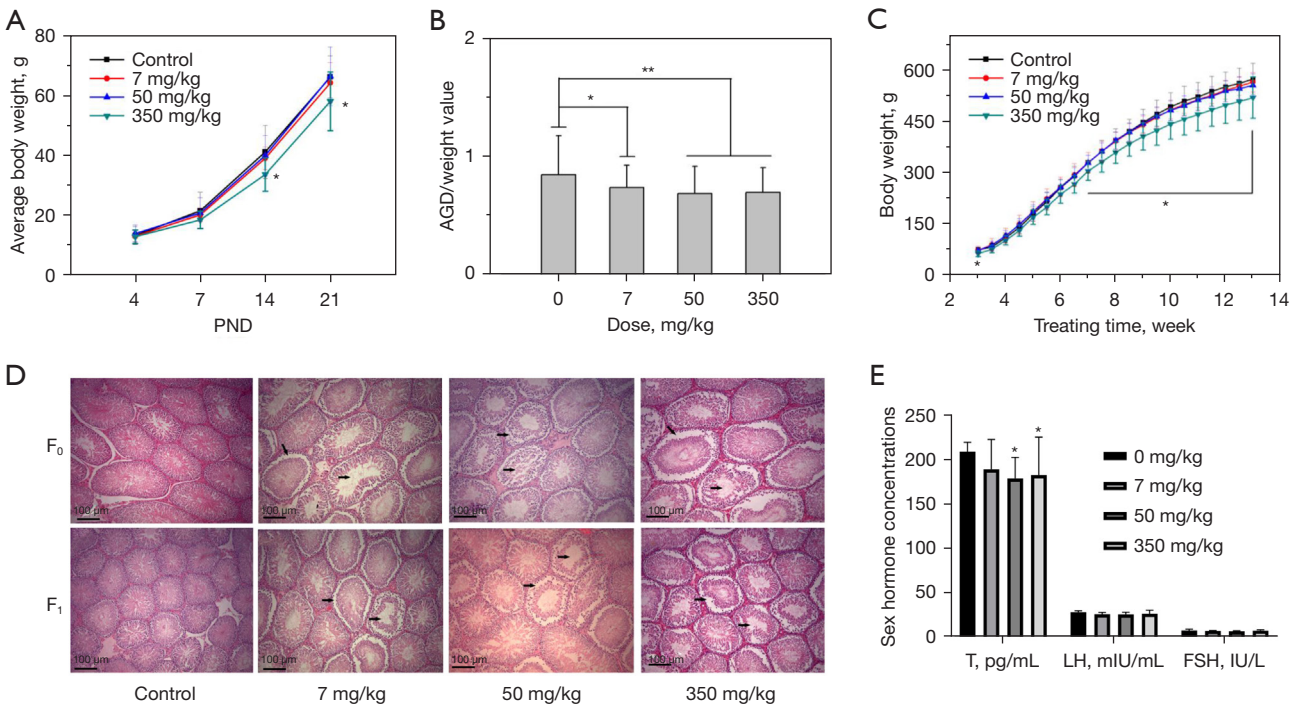

Figure 5 F_1 generation developmental and reproductive toxicity assessments. (A) Average bodyweight of F_1 offspring male rats during lactation. (B) AGD of offspring male rats exposed to ZnO NPs. (C) Body weight of offspring male rats after weaning continuous exposure ZnO NPs. (D) Light microscopy of cross-sections of HE-stained testes from parent and offspring male SD rats (×200). The black arrows indicate the pathological injuries caused by ZnO NPs in testis tissues, such as exfoliation from base membrane, disarrangement of spermatogenic cells, and decreased numbers of the germ cells. (E) Hormone levels (T, LH and FSH) in serum of offspring male rats detected by ELISA. Statistical significance is represented as *P<0.05 and **P<0.01 as compared with control group. AGD, anogenital distance; ZnO NPs, zinc oxide nanoparticles; HE, hematoxylin and eosin; SD, Sprague-Dawley; ELISA, enzyme-linked immunosorbent assay. T, testosterone; LH, luteinizing hormone; FSH, follicle-stimulating hormone.

significantly lower than the control group (P<0.05) (*Table 1*).

ZnO NPs induced dose-dependent changes in cell viability in vitro

The particle size distribution of 20 μg/mL ZnO NPs with DLS determination demonstrated that ZnO NPs have a certain degree of agglomeration, but they could still be maintained in a smaller particle size range and the Zeta potentials were all negative. In addition, the stability was good within 7 days, which was suitable for carrying out follow-up research experiments (Table S3 and Figure S1).

The cytotoxic effects are shown in *Figure 6A*; the cell viability of C18-4 cells at 0.5 μg/mL was significantly lower than in the control group after 24 hours of exposure with ZnO NPs (P<0.05). However, because the cell density was greater than 90% in 48 hours, the growth of the control group was inhibited. Therefore, the significant decrease in cell viability only appeared in the groups above 2.5 μg/mL (P<0.05). After 24 hours of TM4 cell exposure, compared with the control group, the cell viabilities of the 1 and 5 μg/mL groups were significantly reduced. In comparison, only the 5 μg/mL group exhibited a significant decrease after 48 hours (P<0.05) (*Figure 6B*). After TM3 cells had been treated with 10 μg/mL for 24 and 48 hours, the cell viability of each group was significantly lower than in the control group (P<0.05) (*Figure 6C*). The IC_{50} of C18-4 cells were 1.78 and 3.56 μg/mL at 24 and 48 hours, respectively; 1.08 and 1.26 μg/mL for TM4 cells, respectively, and 12.15 and 10.08 μg/mL for TM3 cells, respectively. Thus, among these 3 testicular cells, ZnO NPs was most toxic to the TM4 cells.

In addition, to study whether the high toxicity of ZnO to TM4 cells was due to the size of ZnO, this experiment used ZnO NPs and micro ZnO to poison TM4 cells. As

Table 3 F_1 generation (Cohort 1A)—male organ weight and relative organ coefficient

Test Items	ZnO NPs (mg/kg bw/d)			
	0	7	50	350
Final body weight (mean ± SD, g)	604±52	594±31	576±40	533±62*
Organ weight (mean ± SD, g)				
Liver	16.27±1.85	15.81±1.40	15.53±2.05	14.46±2.04*
Heart	2.01±0.13	1.85±0.14	1.85±0.19	1.73±0.22*
Spleen	1.05±0.18	1.10±0.15	1.05±0.15	0.87±0.18*
Lung	2.32±0.41	2.31±0.25	2.33±0.60	1.92±0.39
Kidney	4.02±0.40	3.77±0.36	3.77±0.47	3.56±0.45*
Brain	2.18±0.12	2.15±0.16	2.14±0.11	2.00±0.18*
Testis	3.69±0.66	3.80±0.37	3.85±0.42	3.28±0.60*
Epididymis	2.14±0.50	1.96±0.57	2.07±0.42	1.95±0.48*
Organ coefficient (mean ± SD, %)				
Liver	2.69±0.16	2.66±0.19	2.69±0.25	2.72±0.33
Heart	0.33±0.03	0.31±0.02	0.32±0.03	0.33±0.03
Spleen	0.17±0.03	0.18±0.02	0.18±0.03	0.16±0.03
Lung	0.39±0.07	0.39±0.04	0.41±0.11	0.36±0.07
Kidney	0.67±0.04	0.63±0.05	0.65±0.07	0.67±0.09
Brain	0.36±0.03	0.36±0.03	0.37±0.03	0.38±0.05
Testis	0.61±0.10	0.64±0.06	0.67±0.06	0.62±0.13
Epididymis	0.36±0.09	0.33±0.10	0.36±0.08	0.37±0.10

Statistical significance is represented as *P<0.05 as compared with control group. ZnO NPs, zinc oxide nanoparticles.

shown in *Figure 6D*, the synapses of TM4 cells disappeared, and the cells became round, fell off, and were suspended in the culture medium after exposure to ZnO NPs and micro ZnO. After 24 hours of exposure to 10 μg/mL ZnO NPs, the viability of TM4 cells reduced to less than 50% of the control group (P<0.05), while the same dose of micro ZnO had almost no effects on the cells (*Figure 6E*). After 48 hours of 10 μg/mL micro ZnO exposure, the TM4 cell viability was significantly reduced, but compared with the same dose of ZnO NPs, the cell viability was significantly increased (P<0.05).

Effects of ZnO NPs on the number and morphology of TM4 cell nuclei

We performed HCA imaging analysis to analyze the nuclear morphology, number, and image intensity of TM4 cells. As shown in *Figure 7A*, the nuclei of ZnO NPs exposure groups showed the increased nuclear area and intensity, and decreased nuclear number at 24 and 48 hours of treatment. The analysis results of each cell in 49 fields per well showed that 1 and 1.25 μg/mL ZnO NPs could significantly reduce the number of cell nuclei (P<0.05), which was basically consistent with the cell viability results (*Figure 7B*). Compared with the control group, the nuclear area and intensity of the 0.2–1.25 μg/mL group increased significantly (P<0.05) (*Figure 7C,7D*). In addition, ZnO NPs had no significant effect on the parameters of nuclear shape (P2A and LWR) (P>0.05) (Table S4).

In addition, we used γ-H2AX labeling to analyze DNA damage responses. The morphology of antibody labeling showed that 1.25 μg/mL ZnO NPs could significantly increase the γ-H2AX positive cells (*Figure 7A*). Furthermore, the γ-H2AX positive cells increased in a dose-

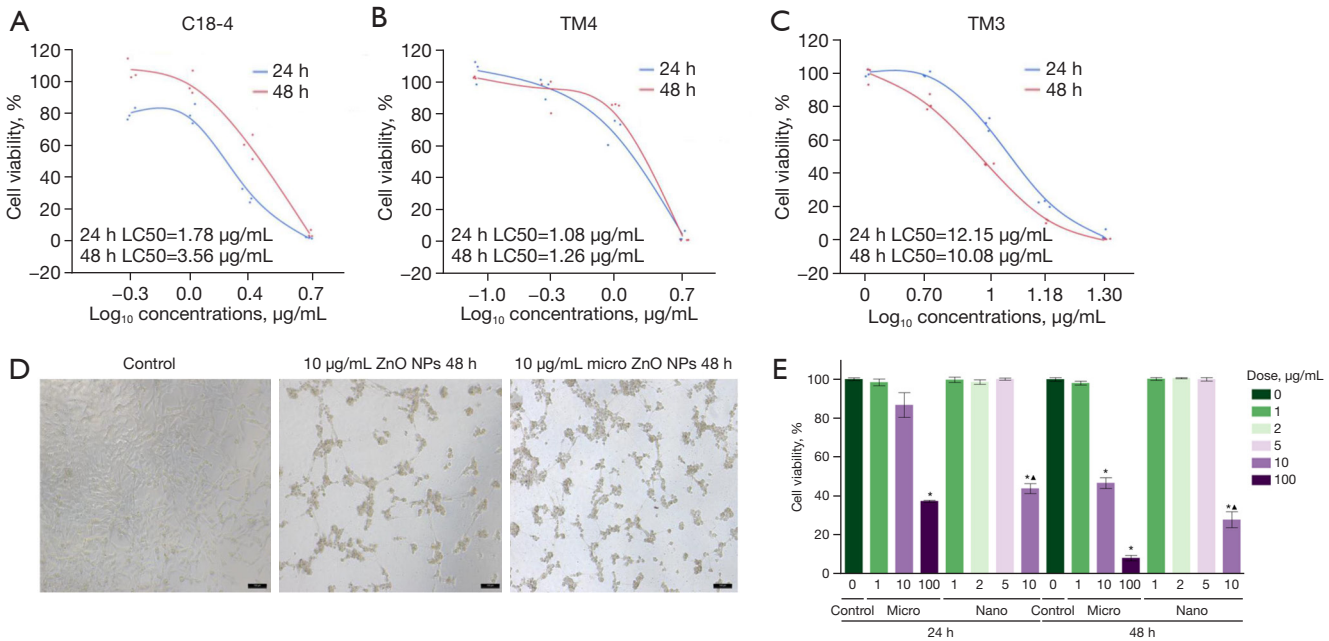

Figure 6 Exposure of ZnO NPs reduced cell viability *in vitro*. (A-C) NR assay for determination of ZnO NPs in C18-4, TM4, and TM3 cells. (D) Effects of ZnO NPs and micro ZnO on the morphology of TM4 cells (×200). (E) Cytotoxic analysis of TM4 cells upon ZnO NPs and micro ZnO treatments after 24 h and 48 h. Statistical significance is represented as *P<0.05 and *▲P<0.01 as compared with control group. ZnO NPs, zinc oxide nanoparticles; NR, neutral red.

dependent manner, and the 1 and 1.25 μg/mL ZnO NPs groups had significant elevation compared with the control group (P<0.05) (*Figure 7E*).

Effects of ZnO NPs on BTB-related proteins

The results of F-actin and Arp3 changes after ZnO NPs exposure showed that F-actin constricted and unwound, concentrated around the nucleus, and the connections between cells had basically disappeared after treatment with ZnO NPs (*Figure 8*). Moreover, the expression of Arp3 only surrounded the nucleus. Compared with the control group, the total intensity of F-actin and Arp3 increased significantly (P<0.05), but the values of entropy and angular second moment decreased significantly (P<0.05), which further indicates that ZnO NPs could change the distribution of actin and its related proteins in cells (*Figure 8B,8D*).

Interestingly, LC3B was basically not expressed in the control group, but it was significantly expressed after exposure to ZnO NPs (P<0.05) (*Figure 8C*). The intercellular substance of α-tubulin was reduced significantly (P<0.05), and it was mainly concentrated around the nucleus (*Figure 8F*). The total intensities of α-tubulin and LC3B were significantly higher than those in the control group (P<0.05), but the values of entropy and mean intensity of α-tubulin were significantly reduced (P<0.05), which further indicates that ZnO NPs could change the content and distribution of tubulin and its related proteins in cells (*Figure 8C,8E*).

To further clarify the relationship between the 4 proteins related to the structure and function of BTB in this study, we used the total intensity value to analyze their pairwise correlation. *Figure 8G* demonstrates that as the exposure dose increased, the correlation between LC3B and F-actin and Arp3 became stronger. These results suggested that ZnO NPs might induce the change of actin through the alteration of LC3B.

Discussion

With the widespread application of ZnO NPs in daily human life, their potential impacts on the human body, especially the male reproductive system, have attracted increasing attention. Therefore, we conducted a ZnO NPs exposure experiment on parental and offspring SD rats in order to derive the possible mechanism of ZnO NPs on the reproductive system. During the ZnO NPs exposure

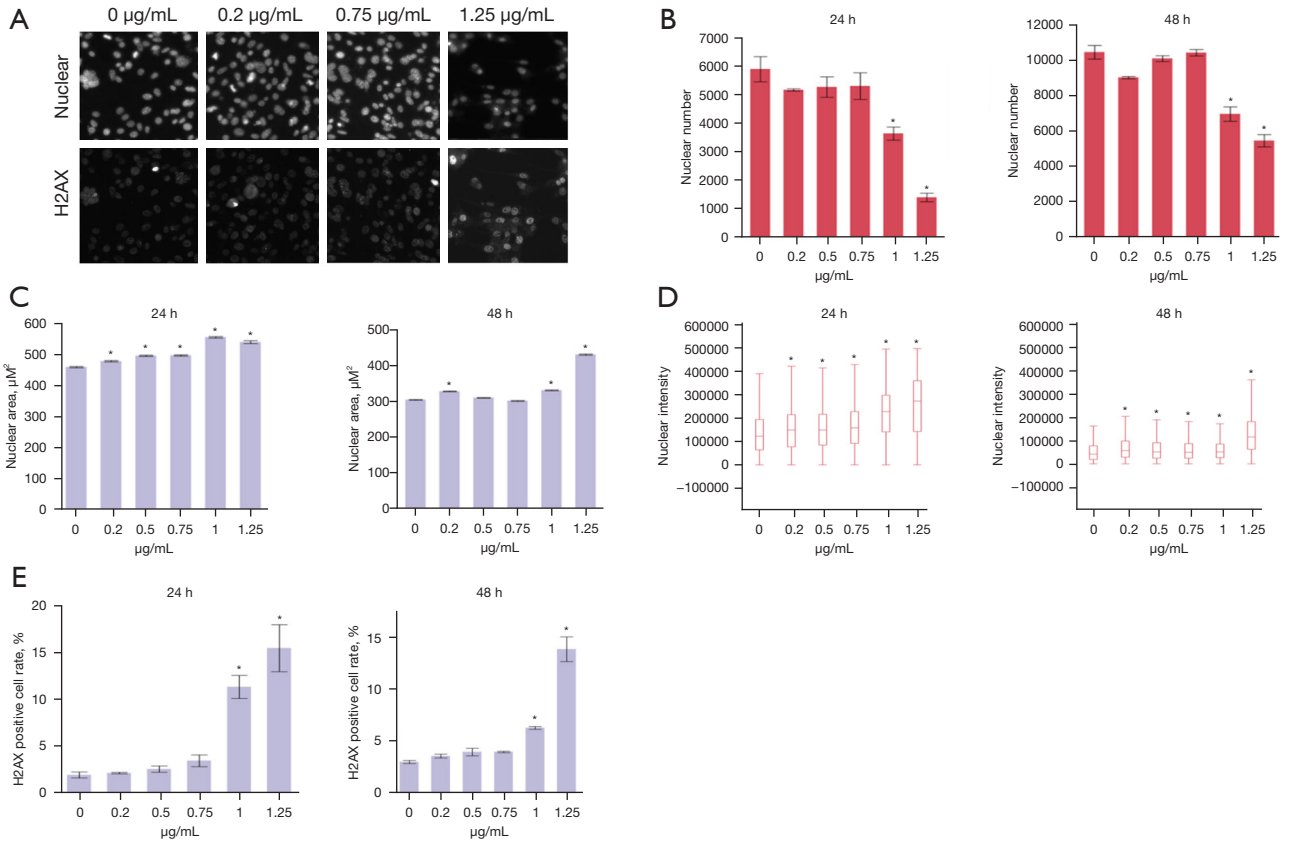

Figure 7 Effects of ZnO NPs on the number and morphology of TM4 cell nuclei. (A) Effects of ZnO NPs on the morphology of TM4 cell nucleus by immunocytochemistry (×400). Effects of ZnO NPs on the number (B), area (C) and total intensity (D) of TM4 cell nucleus. (E) Effects of ZnO NPs on the positive rate of γ-H2AX. Statistical significance is represented as *P<0.05 as compared with control group. ZnO NPs, zinc oxide nanoparticles.

period, there were no abnormal symptoms such as vomiting, diarrhea, cloudy eyes in both control and ZnO NPs-treated male rats. Furthermore, throughout the experimental period, the weight gain of rats in the 350 mg/kg ZnO NPs group gradually slowed down, but there was no significant difference compared with the control group (*Figure 3A*). This was similar to the weight gain result of SD rats treated with different doses of ZnO NPs (0, 50, 150, 450 mg/kg) for 14 days (25). We also found that ZnO NPs entered the human body through different methods and reached various tissues, and most of them were concentrated in the kidney, liver, and lungs (26-28). In the present study, we showed that rats were given 20 nm zinc oxide by oral gavage, and the content of zinc in the liver and testis of 350 mg/kg ZnO NPs group was significantly higher than in the control group, which indicates that the liver served as the main metabolic organ and then entered the target organs after oral administration of ZnO NPs. The contents of total zinc in the testes of the 7 and 50 mg/kg dose groups were almost the same as the control group, and there was no clear dose relationship. The reason may be that the sample was taken 24 hours after the last gavage. Choi *et al.* demonstrated that after oral exposure ZnO NPs for 6 hours in mice, the low concentration of small particles of nanomaterials in the organs could be removed (29). At the same time, it was further shown that the testis was a toxic organ of ZnO NPs rather than an accumulating organ. In addition, the suspected particles found in the testicular electron microscope observation were confirmed to contain zinc and oxygen by EDX analysis (*Figure 4C*), which showed that after oral administration of ZnO NPs in rats, they would be distributed in the organs as a prototype, which caused us to speculate that ZnO NPs can produce potential toxic effects in the testis tissue.

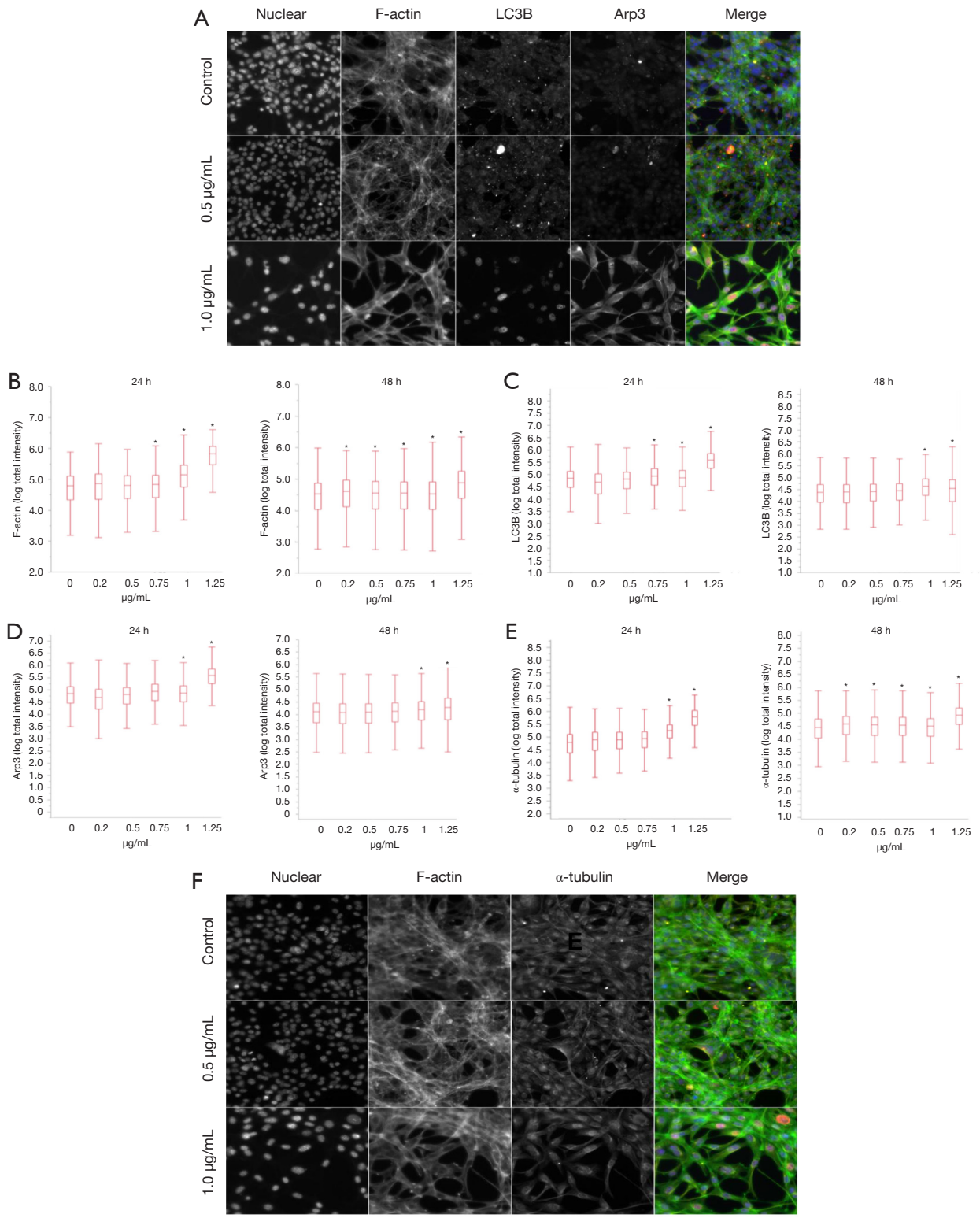

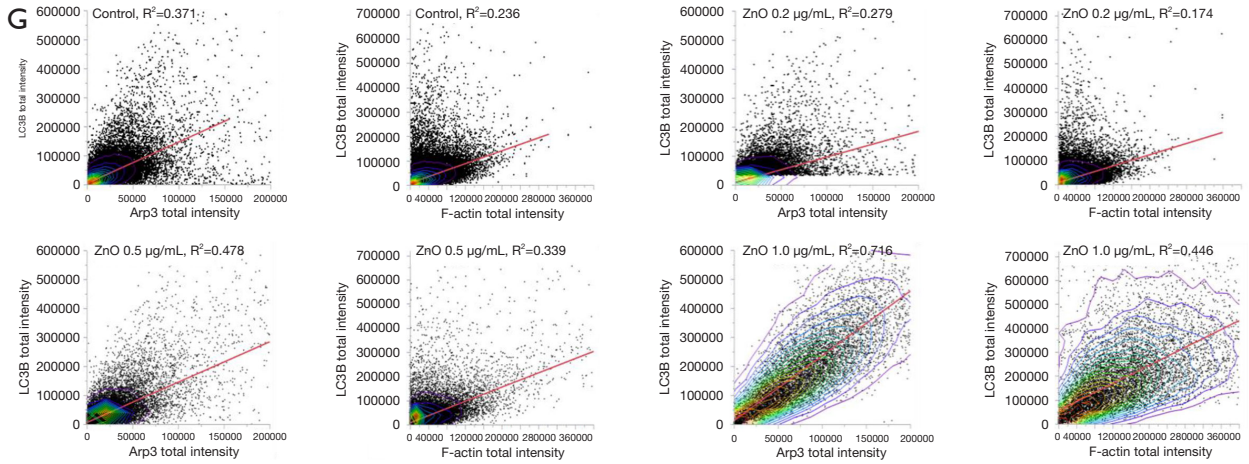

Figure 8 Effects of ZnO NPs on actin, tubulin, and their related proteins. (A) Expression of F-actin, LC3B, and Arp3 were examined by immunofluorescence after exposure of TM4 cells to ZnO NPs. (B-E) The values of F-actin, Arp3, LC3B, α-tubulin, and distribution-related entropy and mean intensity were significantly reduced. (F) Expression of α-tubulin was examined by immunofluorescence after exposure of TM4 cells to ZnO NPs. (G) BTB protein correlation analysis. ZnO NPs, zinc oxide nanoparticles; BTB, blood-testis barrier.

In the present study, we found that ZnO NPs can reduce the weights of liver, testis, and epididymis of paternal (*Figure 3B*,*3C*) and offspring (*Table 3*) male rats, which indicates that the ZnO NPs may be toxic to organs and cause degeneration of the male reproductive organs. Previous studies have shown that the accumulation of nanoparticles has adverse effects on the testis, including lesions in the testicular tissue, sperm abnormalities, and changes in serum sex hormone levels (25,30). The histopathological examination results of testis showed that ZnO NPs caused damage to the testis in a time- and dose-dependent manner (the pathological changes of the offspring's testicular tissue were more severe than those of the parent), including mitochondrial swelling, nuclear damage, and then secondary autophagy and cell deaths. In addition, spermatogenic cells fell off into the lumen and produced a large number of megakaryocytes, which could allow immature or abnormal sperm cells to enter the testicular network, which affected the vitality and morphology of sperm (*Figure 4E*). We also found that the motility and count of parental and offspring sperm were significantly reduced in a dose-dependent manner and the number of sperm deaths was significantly increased (*Tables 1*,*2*), but the number of spermatogenic cells in each stage of the parental testis was not substantially different from that of the control group (P>0.05) (*Figure 4E*). However, the morphology of sperm appeared disorderly and supportive of cell vacuolation. Long-shaped spermatids were retained in the seminiferous epithelium during the developmental stages VII-VIII (*Figure 4D*), which indicates that ZnO NPs could inhibit the spermatogenesis of the spermatogenic epithelium of male rats.

Testosterone is necessary for spermatogenesis, and FSH and LH act in an indirect paracrine fashion to regulate spermatogenesis (31,32). Testosterone can promote meiotic progression (33), and its loss leads to changes in proteins with functions in DNA repair, cell signaling, apoptosis, and meiosis (34). Our study showed that the levels of T, LH, and FSH in the parental 350 mg/kg decreased in a dose-dependent manner, and the levels of LH and FSH in the 350 mg/kg group decreased were significantly lower than in the control group (P<0.05) (*Figure 4G*). After exposure to ZnO NPs, the serum T levels in the offspring of 7 mg/kg and 50 mg/kg groups decreased, which was significantly different from that of the control group (P<0.05) (*Figure 5E*). The changes of the 3 hormones to varying degrees and the changes in sperm quantity and quality all indicate that ZnO NPs can interfere with the secretion of androgens. However, the results in the parent and offspring rats were inconsistent, which may be related to the fact that the serum hormone levels did not completely reflect the testosterone level. The effects of ZnO NPs on the reproductive ability of male rats showed that under the condition that the sperm motility of parental rats was significantly changed, there was no change in the conception rate and pregnancy rate related to the exposure

of ZnO NPs (*Tables 1*,*2*). However, in the experimental results of offspring rats, the conception rate and pregnancy rate in the 350 mg/kg group decreased, accompanied by a decrease in sperm counts in the 7 and 50 mg/kg groups. At the same time, during the development of the offspring male rats, the average body weight of male rats were significantly lower than that of the control group (*Figure 5A*), and the AGD of the offspring rats 4 days after birth was significantly shortened in a dose-dependent manner (*Figure 5B*). The above results suggested that early and long-term ZnO NPs exposure can affect the reproductive ability of male rats.

To further explore the mechanism of ZnO NPs on testicular damage, we established different testicular cell models *in vitro* to study the toxic effects of ZnO NPs on testicular cells, identify the most sensitive cells, and find the possible mechanism on the spermatogenesis of testis. Spermatogenesis is mainly regulated by Leydig cells, Sertoli cells, and peritubular myoid cells (PTM) (32). Sertoli cells (TM4) play a key role in spermatogenesis by providing nutritional support and physical support to germ cells (35). Leydig cells (TM3) are involved in the secretion of androgens and play a key role in meiosis and sperm formation, thereby participating in spermatogenesis (32,36). The PTM cells help coordinate spermatogenesis, and their structure and function can be changed when spermatogenesis is abnormal (32). Furthermore, we also established an *in vitro* model of spermatogonial (C18-4) cell lines. The C18-4 lines show the morphological characteristics of type A spermatogonial cells and express germ cell-specific proteins, which can be used as *in vitro* cell model to assess testicular toxicity and identify testicular signaling pathways (37,38). In the present study, the results showed that ZnO NPs exerted obviously cytotoxic effects on C18-4, TM3, and TM4 cells (*Figure 6A-6C*). However, compared with the toxicity results of ZnO NPs on GC2-spd spermatogonial cell lines and TM4 cells carried out by Liu *et al.* (16), the toxicity of this experiment was more significant. This may be because the nanoparticles in the culture medium of this experiment had small particle sizes and large negative surface charge, which made it easier for ZnO NPs to enter cells and cause severe cytotoxicity. The results also showed that TM4 cells were more sensitive to ZnO NPs. To further determine the toxicity of ZnO NPs, we also compared the toxicity of ZnO NPs and micro-ZnO to TM4 cells (*Figure 6E*). The results showed that the effect of ZnO NPs on TM4 cell viability was higher than that of micron ZnO at the same concentration, which can further clarify that the toxicity of ZnO to testicular cells was not only due to the release of zinc ions, but also included the damage caused by the direct entry of small nanoparticles into cells.

Sertoli cells are located on the basement membrane (39) and their surface is composed of tight junction proteins associated with BTB (40), which help prevent the passage of macromolecules and provide a favorable microenvironment for healthy sperm cell development (41). In the *in vivo* experiment, it was found that Sertoli cells in the testis of male rats vacuolated after ZnO NPs was exposed to SD rats for 70 days (*Figure 4A*). At the same time, it was found that the Sertoli cell viability was affected at the concentration of 1 μg/mL in the *in vitro* experiments (*Figure 6B*). Therefore, we further evaluated the toxicity of ZnO NPs to Sertoli cells by nuclear morphology and DNA damage. The results of HCA showed that TM4 cells were treated with ZnO NPs for 24 and 48 hours, nuclear area and nuclear strength were significantly increased, but there were no significant changes observed regarding P2A and LWR. In addition, 0.2 μg/mL ZnO NPs induced a decrease in cell number that was lower than that observed by NR assay (*Figure 7B-7D*). These results indicated that ZnO NPs could induce changes in the number and morphology of Sertoli cell nuclei. The detection of γ-H2AX has been identified as an early and sensitive cell biomarker of DNA damage (42,43). Sharma *et al.* (44) and Lai *et al.* (45) showed that ZnO NPs can induce intracellular oxidative stress, which usually leads to DNA damage. Therefore, we further evaluated the damage caused by ZnO NPs to Sertoli cells by detecting the expression level of γ-H2AX protein. We found that the expression level of γ-H2AX was significantly changed by ZnO NPs, and the number of γ-H2AX positive cells was increased when the concentration of ZnO NPs reached 1 μg/mL (*Figure 7E*). The number of γ-H2AX-positive cells in the 1.25 μg/mL group was 5 times and 5.5 times higher than that in the control group at 24 and 48 hours after exposure, respectively (*Figure 7E*). These results suggest that the genotoxic effects of ZnO NPs on germ cells can be observed by increasing the expression of the DNA damage response marker γ-H2AX. Daoud *et al.* showed that ZnO NPs, at their investigated doses and given their properties (10 mg/kg/BW), exerted an ameliorative effect against benzo[α]pyrene by decreasing oxidative stress and by increasing the expression levels of steroidogenic enzymes, resulting in the repair of tissue abnormalities (46). And Anan *et al.* showed that ZnO NPs effectively ameliorate the deleterious histological and biochemical

changes induced by cyclophosphamide in rat testis through their antioxidant and anti-apoptotic effects (47). In fact, the effects of ZnO NPs depend on their size, concentration, morphology, and surface area. Abbasalipourkabir *et al.* indicated that the significant toxicity effects of ZnO NPs appeared at concentrations above 50 mg/kg body weight of animals (48). At low concentrations, ZnO NPs act as antioxidants, while they produce ROS and induce apoptosis at high concentrations (20).

The BTB is formed by actin tight junctions (TJ) and gap junctions (GJ) at the bottom of spermatogenic epithelium between adjacent Sertoli cells near the basement membrane (49). In addition, the cytoskeleton of actin and microtubules (MT) is essential for maintaining BTB homeostasis and has been identified as a primary target of some reproductive toxicants, which may lead to toxic reproductive effects (50,51). As a mechanism of actin nucleation and branching, the Arp2/3 complex is abundantly present in the lamellar pseudopodia on the front edge of motor cells, which contains branched-chain actin filaments (52). In this study, HCA combined with high-throughput image analysis results showed that after TM4 cells were treated with ZnO NPs, Arp3 moved across the cell-cell interface into the cell cytoplasm, and F-actin was withdrawn from the cell cytoplasm, distributed around the nucleus, and formed a ring (*Figure 8A*). In addition, the expression intensity of F-actin and Arp3 was significantly higher than that of the control group, but the values of entropy and angular second moment were significantly reduced, which suggested that ZnO NPs can affect the morphology and distribution of actin and Arp3, thereby interfering with the structure and function of actin-based cytoskeleton (*Figure 8B*,*8D*).

As a track to transport organelles MT is used to transport developing germ cells (53). Microtubule-associated protein 1 light chain 3B (LC3B) (54) is a marker protein for autophagy detection, which exists on microfilaments. The image morphology results showed that the distribution of α-tubulin was recovered from the cytoplasm to the nucleus of the cells treated with ZnO NPs, and the expression level of LC3B increased significantly with the exposure of ZnO NPs. Compared with the control group, the total intensity of α-tubulin and LC3B increased significantly, but the values of entropy and mean intensity related to the distribution of α-tubulin decreased significantly, which further indicates that ZnO NPs can change the content and distribution of tubulin and its related proteins in cells (*Figure 8C*,*8E*). We aimed to study the synergistic effect of actin- and MT-based cytoskeleton, as well as the role of related regulatory proteins. The correlation analysis of the protein expression of F-actin, Arp3, α-tubulin and LC3B after ZnO NPs exposure showed that with the increase of the exposure dose, the correlation between LC3B and F-actin, LC3B, and Arp3 all increased significantly, which inferred that ZnO NPs can affect the expression of LC3B protein and then have an effect on microfilament protein and actin, thereby disturbing the dynamic balance of BTB (*Figure 8G*).

Conclusions

Based on the results from the above *in vivo* and *in vitro* experiments, we hypothesized the underlying mechanism of ZnO NPs-induced testicular toxicity. ZnO NPs can directly damage the integrity of the testicular tissue structure, penetrate the BTB into the seminiferous epithelium of the testis, and directly act on the Sertoli cells of the testis to disturb its structure and physiological processes. It destroys the dynamic balance of the BTB, damages the cytoskeleton, and disrupts the dynamic balance of BTB. After the disruption of BTB, ZnO NPs enter the seminiferous epithelium and directly act on the spermatogenic cells, which leads to the programmed death of spermatogenic cells. The number of sperm deaths increases and a certain degree of sperm deformity occurs. In addition, it is also considered that ZnO NPs may cause damage to interstitial cells and dysregulate T synthesis and secretion; thereby, the Sertoli cells and seminiferous epithelium cannot function normally, aggravate the reduction of sperm count and sperm motility, and ultimately affect the reproductive ability of rats.

Acknowledgments

Funding: This study was supported by the three-year action plan of Shanghai public health system construction (No. GWTD2015S03).

Footnote

Reporting Checklist: The authors have completed the ARRIVE reporting checklist. Available at https://atm.amegroups.com/article/view/10.21037/atm-22-3047/rc

Data Sharing Statement: Available at https://atm.amegroups.

com/article/view/10.21037/atm-22-3047/dss

Conflict of Interest: All authors have completed the ICMJE uniform disclosure form (available at https://atm.amegroups.com/article/view/10.21037/atm-22-3047/coif). LY is from Reprotox Biotech LLC. The other authors have no conflicts of interest to declare.

Ethical Statement: The authors are accountable for all aspects of the work in ensuring that questions related to the accuracy or integrity of any part of the work are appropriately investigated and resolved. Animal experiments were performed in accordance with the Guide for the Care and Use of Laboratory Animals. The animal experiment protocol was reviewed and approved by the Animal Ethics Review Committee of the Shanghai Municipal Center for Disease Control and Prevention.

References

1. El-Shorbagy HM, Eissa SM, Sabet S, et al. Apoptosis and oxidative stress as relevant mechanisms of antitumor activity and genotoxicity of ZnO-NPs alone and in combination with N-acetyl cysteine in tumor-bearing mice. Int J Nanomedicine 2019;14:3911-28.
2. Kalpana VN, Devi Rajeswari V. A Review on Green Synthesis, Biomedical Applications, and Toxicity Studies of ZnO NPs. Bioinorg Chem Appl 2018;2018:3569758.
3. Sekhon BS. Nanotechnology in agri-food production: an overview. Nanotechnol Sci Appl 2014;7:31-53.
4. Oberdörster G, Maynard A, Donaldson K, et al. Principles for characterizing the potential human health effects from exposure to nanomaterials: elements of a screening strategy. Part Fibre Toxicol 2005;2:8.
5. de Braganca L, Ferguson GJ, Luis Santos J, et al. Adverse immunological responses against non-viral nanoparticle (NP) delivery systems in the lung. J Immunotoxicol 2021;18:61-73.
6. Hackenberg S, Scherzed A, Harnisch W, et al. Antitumor activity of photo-stimulated zinc oxide nanoparticles combined with paclitaxel or cisplatin in HNSCC cell lines. J Photochem Photobiol B 2012;114:87-93.
7. Pujalté I, Passagne I, Brouillaud B, et al. Cytotoxicity and oxidative stress induced by different metallic nanoparticles on human kidney cells. Part Fibre Toxicol 2011;8:10.
8. Park HS, Shin SS, Meang EH, et al. A 90-day study of subchronic oral toxicity of 20 nm, negatively charged zinc oxide nanoparticles in Sprague Dawley rats. Int J Nanomedicine 2014;9 Suppl 2:79-92.
9. Pinho AR, Martins F, Costa MEV, et al. In Vitro Cytotoxicity Effects of Zinc Oxide Nanoparticles on Spermatogonia Cells. Cells 2020;9:1081.
10. Prasad AS, Bao B. Molecular Mechanisms of Zinc as a Pro-Antioxidant Mediator: Clinical Therapeutic Implications. Antioxidants (Basel) 2019;8:164.
11. Bisht G, Rayamajhi S. ZnO Nanoparticles: A Promising Anticancer Agent. Nanobiomedicine (Rij) 2016;3:9.
12. Erfani Majd N, Hajirahimi A, Tabandeh MR, et al. Protective effects of green and chemical zinc oxide nanoparticles on testis histology, sperm parameters, oxidative stress markers and androgen production in rats treated with cisplatin. Cell Tissue Res 2021;384:561-75.
13. Liu J, Kang Y, Yin S, et al. Zinc oxide nanoparticles induce toxic responses in human neuroblastoma SHSY5Y cells in a size-dependent manner. Int J Nanomedicine 2017;12:8085-99.
14. Choudhury SR, Ordaz J, Lo CL, et al. From the Cover: Zinc oxide Nanoparticles-Induced Reactive Oxygen Species Promotes Multimodal Cyto- and Epigenetic Toxicity. Toxicol Sci 2017;156:261-74.
15. Han Z, Yan Q, Ge W, et al. Cytotoxic effects of ZnO nanoparticles on mouse testicular cells. Int J Nanomedicine 2016;11:5187-203.
16. Liu Q, Xu C, Ji G, et al. Sublethal effects of zinc oxide nanoparticles on male reproductive cells. Toxicol In Vitro 2016;35:131-8.
17. Rafiee Z, Khorsandi L, Nejad-Dehbashi F. Protective effect of Zingerone against mouse testicular damage induced by zinc oxide nanoparticles. Environ Sci Pollut Res Int 2019;26:25814-24.
18. Bara N, Kaul G. Enhanced steroidogenic and altered antioxidant response by ZnO nanoparticles in mouse testis Leydig cells. Toxicol Ind Health 2018;34:571-88.
19. OECD. Test No. 443: Extended One-Generation Reproductive Toxicity Study2018. Available online: https://www.oecd.org/chemicalsafety/test-no-443-extended-one-

generation-reproductive-toxicity-study-9789264185371-en.htm
20. Pinho AR, Rebelo S, Pereira ML. The Impact of Zinc Oxide Nanoparticles on Male (In)Fertility. Materials (Basel) 2020;13:849.
21. Albus U. Guide for the Care and Use of Laboratory Animals (8th edn). Laboratory Animals 2012;46:267-8.
22. Ichihara G, Yu X, Kitoh J, et al. Reproductive toxicity of 1-bromopropane, a newly introduced alternative to ozone layer depleting solvents, in male rats. Toxicol Sci 2000;54:416-23.
23. Turnbull D, Jack MM, Coder PS, et al. Extended One-Generation Reproductive Toxicity (EOGRT) study of benzoic acid in Sprague Dawley rats. Regul Toxicol Pharmacol 2021;122:104897.
24. Liang S, Yin L, Shengyang Yu K, et al. High-Content Analysis Provides Mechanistic Insights into the Testicular Toxicity of Bisphenol A and Selected Analogues in Mouse Spermatogonial Cells. Toxicol Sci 2017;155:43-60.
25. Tang Y, Chen B, Hong W, et al. ZnO Nanoparticles Induced Male Reproductive Toxicity Based on the Effects on the Endoplasmic Reticulum Stress Signaling Pathway. Int J Nanomedicine 2019;14:9563-76.
26. Lee CM, Jeong HJ, Yun KN, et al. Optical imaging to trace near infrared fluorescent zinc oxide nanoparticles following oral exposure. Int J Nanomedicine 2012;7:3203-9.
27. Li CH, Shen CC, Cheng YW, et al. Organ biodistribution, clearance, and genotoxicity of orally administered zinc oxide nanoparticles in mice. Nanotoxicology 2012;6:746-56.
28. Choi SJ, Choy JH. Biokinetics of zinc oxide nanoparticles: toxicokinetics, biological fates, and protein interaction. Int J Nanomedicine 2014;9 Suppl 2:261-9.
29. Choi J, Kim H, Kim P, et al. Toxicity of zinc oxide nanoparticles in rats treated by two different routes: single intravenous injection and single oral administration. J Toxicol Environ Health A 2015;78:226-43.
30. Iqbal A, Zakir M, Ali MM, et al. Effects of Allium cepa-mediated zinc oxide nanoparticles on male reproductive tissue and sperm abnormalities of albino mice (Mus musculus). Applied Nanoscience 2021;11:807-15.
31. Huhtaniemi I. A short evolutionary history of FSH-stimulated spermatogenesis. Hormones (Athens) 2015;14:468-78.
32. Zhou R, Wu J, Liu B, et al. The roles and mechanisms of Leydig cells and myoid cells in regulating spermatogenesis. Cell Mol Life Sci 2019;76:2681-95.
33. Haywood M, Spaliviero J, Jimemez M, et al. Sertoli and germ cell development in hypogonadal (hpg) mice expressing transgenic follicle-stimulating hormone alone or in combination with testosterone. Endocrinology 2003;144:509-17.
34. Stanton PG, Sluka P, Foo CF, et al. Proteomic changes in rat spermatogenesis in response to in vivo androgen manipulation; impact on meiotic cells. PLoS One 2012;7:e41718.
35. Qiu L, Zhang X, Zhang X, et al. Sertoli cell is a potential target for perfluorooctane sulfonate-induced reproductive dysfunction in male mice. Toxicol Sci 2013;135:229-40.
36. Shima Y, Miyabayashi K, Haraguchi S, et al. Contribution of Leydig and Sertoli cells to testosterone production in mouse fetal testes. Mol Endocrinol 2013;27:63-73.
37. Oatley JM, Brinster RL. Regulation of spermatogonial stem cell self-renewal in mammals. Annu Rev Cell Dev Biol 2008;24:263-86.
38. Lucas BE, Fields C, Joshi N, et al. Mono-(2-ethylhexyl)-phthalate (MEHP) affects ERK-dependent GDNF signalling in mouse stem-progenitor spermatogonia. Toxicology 2012;299:10-9.
39. El-Behery EI, El-Naseery NI, El-Ghazali HM, et al. The efficacy of chronic zinc oxide nanoparticles using on testicular damage in the streptozotocin-induced diabetic rat model. Acta Histochem 2019;121:84-93.
40. Pelletier RM. The blood-testis barrier: the junctional permeability, the proteins and the lipids. Prog Histochem Cytochem 2011;46:49-127.
41. Johnson L, Thompson DL Jr, Varner DD. Role of Sertoli cell number and function on regulation of spermatogenesis. Anim Reprod Sci 2008;105:23-51.
42. Rogakou EP, Pilch DR, Orr AH, et al. DNA double-stranded breaks induce histone H2AX phosphorylation on serine 139. J Biol Chem 1998;273:5858-68.
43. Nikolova T, Dvorak M, Jung F, et al. The γH2AX assay for genotoxic and nongenotoxic agents: comparison of H2AX phosphorylation with cell death response. Toxicol Sci 2014;140:103-17.
44. Sharma V, Singh P, Pandey AK, et al. Induction of oxidative stress, DNA damage and apoptosis in mouse liver after sub-acute oral exposure to zinc oxide nanoparticles. Mutat Res 2012;745:84-91.
45. Lai X, Wei Y, Zhao H, et al. The effect of Fe2O3 and ZnO nanoparticles on cytotoxicity and glucose metabolism in lung epithelial cells. J Appl Toxicol 2015;35:651-64.
46. Daoud NM, Aly MS, Ezzo OH, et al. Zinc oxide nanoparticles improve testicular steroidogenesis machinery

dysfunction in benzo[α]pyrene-challenged rats. Sci Rep 2021;11:11675.
47. Anan HH, Zidan RA, Abd El-Baset SA, et al. Ameliorative effect of zinc oxide nanoparticles on cyclophosphamide induced testicular injury in adult rat. Tissue Cell 2018;54:80-93.
48. Abbasalipourkabir R, Moradi H, Zarei S, et al. Toxicity of zinc oxide nanoparticles on adult male Wistar rats. Food Chem Toxicol 2015;84:154-60.
49. Wen Q, Tang EI, Li N, et al. Regulation of Blood-Testis Barrier (BTB) Dynamics, Role of Actin-, and Microtubule-Based Cytoskeletons. Methods Mol Biol 2018;1748:229-43.
50. O'Donnell L, O'Bryan MK. Microtubules and spermatogenesis. Semin Cell Dev Biol 2014;30:45-54.
51. O'Donnell L. Mechanisms of spermiogenesis and spermiation and how they are disturbed. Spermatogenesis 2014;4:e979623.
52. Chhabra ES, Higgs HN. The many faces of actin: matching assembly factors with cellular structures. Nat Cell Biol 2007;9:1110-21.
53. Redi C. Sertoli Cells - Methods and Protocols. Eur J Histochem 2019;63:3014.
54. Huang W, Quan C, Duan P, et al. Nonylphenol induced apoptosis and autophagy involving the Akt/mTOR pathway in prepubertal Sprague-Dawley male rats in vivo and in vitro. Toxicology 2016;373:41-53.

(English Language Editor: J. Jones)

Cite this article as: Hong X, Shao N, Yin L, Li C, Tao G, Sun Y, Qian K, Yang J, Xiao P, Yu X, Zhou Z. Exposure to zinc oxide nanoparticles affects testicular structure, reproductive development and spermatogenesis in parental and offspring male rats. Ann Transl Med 2022;10(13):751. doi: 10.21037/atm-22-3047

